Comparison of different capillary bridge models for application in the discrete element method

Anton Gladkyy* and Rüdiger Schwarze*

* Institute of Mechanics and Fluid Dynamics, TU Bergakademie Freiberg, Lampadiusstr. 4, 09596 Freiberg, Germany.

April 1, 2014

arXiv:1403.7926v1 [cond-mat.soft] 31 Mar 2014

Saturated granular material is the subject of many studies. Several formulations were proposed to calculate the capillary forces between wet particles. Some of such models have been implemented in DEM-framework and simulation results were compared to experimental measurements. Also the influence of capillary model type on macro parameters like local shear viscosity and cohesive parameters of sheared material have been investigated on the DEM-model of split-bottom shear-cell.

It was concluded, that the water content, simulated with the help of capillary bridge models, change the macro-properties of the simulated granular material. But type of capillary bridge model does not influence the macroscopic results visibly.

1 Introduction

Wet granular materials play an important role in geology and many technical applications, e.g. construction, pharmaceuticals, civil engineering, etc. Here, liquid or capillary bridges are present between the granular grains, which produce inter-grain forces on the micro-scale level and drastically modify the mechanical properties of the granular media on the macro-scale levels (e.g. slopes can be much larger than 45 degrees for the banked up wet bulk material) [6, 5, 14].

Such inter-grain capillary forces have been the subject of many investigations within the last several decades, see e. g. [9, 5, 8] for an overview. Modern instruments allow to measure micro- and even nano-scale force values between individual particles very precisely. Based on these experimental information, capillary bridge models (CBM) for capillary force calculations can be deduced, as described e. g. in [7]. Some recent studies in this direction have been done for instance by Willett et al. [23] and Rabinovich et al. [17].

These CBMs can be implemented in particle-based simulation methods, for example on the base of Discrete Element Method (DEM) in order to model the effects of individual capillary bridges between particles. Using a CBM it is possible to simulate the behavior of wetted bulk material and to predict its macro-parameters. This is important for simulations of processes like agglomeration, adhesion, crystallization and others [19, 18, 11].

In this paper we investigate four different kinds of CBMs, which have been frequently used to model capillary bridge forces in DEM simulations. Firstly, the CBM formulations and their implementations in the open-source DEM software package are summarized. Then, the quality of the CBM for the description of individual capillary bridges in the pendular regime (where the capillary bridges exist individually) is tested by comparison of experimental and numerical data. Finally, the every kind of the CBM in simulations of weakly wetted bulk material shear flows is analyzed by cross-comparison of results from the different CBMs. Here, the bridges are again in pendular state.

2 Investigated CBMs

Zhu et al. [24] discuss in their review main features of CBM for the calculation of capillary forces. CBM for application in DEM simulations should consist of easy to implement explicit functions of liquid bridge volume and the particle separation distance. Additionally, the shape of the liquid bridge must be approximated in order to calculate the capillary force.

Two different methods can be adopted: in the

neck (or "gorge") method the force is estimated at the neck of the bridge. Contrary, in the contact (or boundary) method, the force is evaluated at the liquid bridge solid contact region. It has been demonstrated, that the neck method seems to provide the more accurate estimate of capillary force than the contact method [10].

Some recent approaches with explicit CBM functions have been proposed by Weigert and Ripperger [22] (contact method), Willett et al. [23] (neck method), Rabinovich et al. [17] (neck method) and Soulie et al. [21] (neck method). Lambert et al. [8] give a corrected version of Rabinovich's CBM. Several of these CBMs have been already successfully used in DEM simulations of weakly wetted granular material [18, 3, 4, 13, 20]. A comparison of CBMs from Soulie and Rabinovich (with Lambert's correction) has been already given in [3]. Therefore, we will compare all stated CBM except Soulie's in order to identify (i) differences between CBM based on the contact and the neck method and (ii) differences between CBM based on the same method (neck) but with different formulations.

In our study, we apply four different CBMs, which have been proposed in chronological order by Weigert and Ripperger [22], Willett et al. [23] and Rabinovich et al. [17]) for the capillary force F between particles i, j with radii R_i and R_j. In these models, an effective radius R of the particle pair

$$R = \frac{2R_iR_j}{R_i + R_j} \tag{1}$$

is introduced as in Derjaguin's approximation [1]. As constant input parameters, we prescribe the liquid bridge volume $V = V_{bridge}$, the contact angle θ of the liquid-gas interface at the particle surface, and the liquid surface tension γ. In all four CBMs, the distance a between the surfaces of the two particles i, j is the main model variable. We assume, that F (capillary force) is acting only after a normal, mechanical contact between i and j, when an overlap between the particles has already disappeared. F is acting as long as $a < a_{crit}$. The critical distance a_{crit} between two particles is calculated according to Willett et al. [23]:

$$a^*_{crit} = \left(1 + \frac{\theta}{2}\right) \cdot \left(V^{*1/3} + \frac{V^{*2/3}}{10}\right) \tag{2}$$

Where $a^*_{crit} = a_{crit}/R$ and $V^* = V/R^3$ are the dimensionless critical distance and bridge volume accordingly.

All formulations, which are given below, have been implemented in the open-source DEM software Yade [25] in combination with a viscoelastic model for mechanical contacts [16].

2.1 Weigert's model

In the CBM of Weigert and Ripperger [22], simplified equations are employed in order to calculate V and the half-filling angle β from the bulk liquid saturation S. These parameters are needed to calculate F. V_{bridge} can be found as:

$$V = 0.12(2R)^3 \sin^4 \beta C_a C_\theta \tag{3}$$

Since V is a given parameter for us, β can be obtained:

$$\beta = \arcsin\left(\frac{V}{0.12 \cdot (2R)^3 \cdot C_a C_\theta}\right)^{1/4} \tag{4}$$

C_a and C_θ are the correction functions for the distance and the contact angles, respectively, they are calculated according to:

$$C_a = \left(1 + 6\frac{a}{2R}\right) \tag{5}$$

$$C_\theta = (1 + 1.1 \cdot \sin\theta) \tag{6}$$

The capillary pressure p_k is calculated according to the Laplace-Young equation:

$$p_k = \gamma\left(\frac{1}{\hat{R}_1} - \frac{1}{\hat{R}_2}\right) \tag{7}$$

The principal radii of the bridge curvature $\hat{R}_1$ and $\hat{R}_2$ are taken positive and negative, respectively, and calculated according to Pietsch and Rumpf [15]:

$$R_1 = \frac{R(1 - \cos\beta) + a}{\cos(\beta + \theta)} \tag{8}$$

$$R_2 = R\sin\beta + R_1\left[\sin(\beta + \theta) - 1\right] \tag{9}$$

Finally, F is calculated with:

$$F = \frac{\pi}{4}(2R)^2 \sin^2\beta \cdot p_k + \gamma\pi 2R\sin\beta\sin(\beta + \theta) \tag{10}$$

The sequence of equations in implementation is the following: (5), (6), (4), (8), (9), (7), (10).

2.2 Willett's full model

Willett et al. [23] proposed the following CBM, which is based on combined experimental and numerical results, with numerical data from integration of the Laplace-Young equation. The main model variable is the scaled dimensionless half- separation distance S^+:

$$S^+ = \frac{a}{2\sqrt{V/R}} \tag{11}$$

F is calculated from:

$$F = 2\,\pi R\gamma\,\exp(f_1 - f_2\exp(f_3\ln S^+ + f_4\ln^2 S^+)) \tag{12}$$

The coefficients $f_{1\ldots4}$ are calculated as follows:

$$\begin{aligned} f_1 =&(-0.44507 + 0.050832\;\theta - 1.1466\;\theta^2)+\\ &(-0.1119 - 0.000411\;\theta - 0.1490\;\theta^2)\;\ln(V^*)+\\ &(-0.012101 - 0.0036456\;\theta - 0.01255\;\theta^2)\;(\ln(V^*))^2+\\ &(-0.0005 - 0.0003505\;\theta - 0.00029076\;\theta^2)\;(\ln(V^*))^3 \end{aligned} \tag{13}$$

$$\begin{aligned} f2 =&(1.9222 - 0.57473\;\theta - 1.2918\;\theta^2)+\\ &(-0.0668 - 0.1201\;\theta - 0.22574\;\theta^2)\;\ln(V^*)+\\ &(-0.0013375 - 0.0068988\;\theta - 0.01137\;\theta^2)\;(\ln(V^*))^2 \end{aligned} \tag{14}$$

$$\begin{aligned} f3 =&(1.268 - 0.01396\;\theta - 0.23566\;\theta^2)+\\ &(0.198 + 0.092\;\theta - 0.06418\;\theta^2)\;\ln(V^*)+\\ &(0.02232 + 0.02238\;\theta - 0.009853\;\theta^2)\;(\ln(V^*))^2+\\ &(0.0008585 + 0.001318\;\theta - 0.00053\;\theta^2)\;(\ln(V^*))^3; \end{aligned} \tag{15}$$

$$\begin{aligned} f4 =&(-0.010703 + 0.073776\;\theta - 0.34742\;\theta^2)+\\ &(0.03345 + 0.04543\;\theta - 0.09056\;\theta^2)\;\ln(V^*)+\\ &(0.0018574 + 0.004456\;\theta - 0.006257\;\theta^2)\;(\ln(V^*))^2; \end{aligned} \tag{16}$$

The sequence of equations in implementation is the following: (13), (14), (15), (16), (11), (12).

2.3 Willett's reduced model

Willett et al. [23] give also a less complex CBM for equal-sized particles $R_i = R_j = R$. The following equation provides a closed approximation of F between equal-sized spheres:

$$F = \frac{2\,\pi R\gamma\,\cos\theta}{1 + 2.1(S^+) + 10(S^+)^2} \tag{17}$$

Willett et al. [23] noticed, that this expression is valid for $\theta < 50°$ and $V^* < 0.1$. The sequence of equations in implementation is the following: (11), (17).

2.4 Rabinovich's model

Rabinovich et al. [17] give the following CBM, which is based on combined experimental and numerical analysis as well. First of all, the "embracing angle" α for the case sphere-sphere is evaluated:

$$\alpha = \sqrt{\frac{a}{R}\cdot\left(-1 + \sqrt{1 + \frac{2V}{\pi R a^2}}\right)} \tag{18}$$

Then the distance $d_{sp/sp}$ must be found:

$$d_{sp/sp} = \frac{a}{2}\cdot\left[-1 + \sqrt{1 + \frac{2V}{\pi R a^2}}\right] \tag{19}$$

Rabinovich et al. [17]Finally, F is predicted with:

$$F = -\frac{2\pi R\gamma\cos\theta}{1 + \left[a/2d_{sp/sp}\right]} - 2\pi\gamma R\sin\alpha\sin(\theta + \alpha) \tag{20}$$

Later, Lambert et al. [8] identified an error in the deduction of the model and showed, that the second term of equation (20) is redundant. Therefore, we employ Rabinovich's model with Lambert's correction: F is predicted with:

$$F = -\frac{2\pi R\gamma\cos\theta}{1 + \left[a/2d_{sp/sp}\right]} \tag{21}$$

The sequence of equations in implementation is the following: (18), (19), (21).

3 Kinds of investigated CBMs

In a first step different kinds of CBMs are analyzed in predicting individual capillary bridges. Therefore, DEM simulations of a particle pair connected by a single capillary bridge in the pendular regime have been performed. The setup of the simulations correspond to the experiments, which are presented in Willett et al. [23] for micro-scale and in Rabinovich et al. [17] for nano-scale experiments.

Willett et al. [23] employed for the experiments precision synthetic sapphire spheres of radii 2.381, 1.588 and 1.191 mm. In their experiments the liquid bridges are formed of dimethylsiloxane with relevant material parameters surface tension $\gamma = 20.6$ mN/m and contact angle $\theta = 0°$. The liquid bridge volume V has been varied (see Table 1).

Rabinovich et al. [17] used in their study much smaller glass spheres with the radii 19 ... 35 μm. An oil with relevant material parameters γ=[24 ... 28]mN/m and θ = [0 ... 10]° forms the capillary bridges between the particles. Other parameters of the different simulation setups are presented in table 1.

Every of the 13 setups given in table 1 are investigated in DEM simulations using the four CBMs of Weigert et al. (Weig), Willett et al. - full (WilF), Willett et al. - reduced (WilR) and Rabinovich et al. with Lambert's correction (RabL).

In the simulations, two interacting particles touch each other without overlap in their initial positions, i. e. $a = 0$. Then one particle is pulled out with constant velocity whereas the other remains fixed, until the rupture distance of the liquid bridge

Table 1: Setup for DEM-simulations of capillary models, based on Willett's [23] and Rabinovich's [17] experiments

CODE	R_i [mm]	R_j [mm]	γ [mN/m]	θ [°]	V [nl]
W_{11}	2.381	2.381	20.6	0	13.6
W_{12}	-/-	-/-	-/-	-/-	31.3
W_{13}	-/-	-/-	-/-	-/-	74.2
W_{21}	-/-	1.588	-/-	-/-	9.6
W_{22}	-/-	-/-	-/-	-/-	13.2
W_{23}	-/-	-/-	-/-	-/-	24.7
W_{24}	-/-	-/-	-/-	-/-	59.3
W_{31}	-/-	1.191	-/-	-/-	25.3
W_{32}	-/-	-/-	-/-	-/-	61.8
W_{33}	-/-	-/-	-/-	-/-	127.8
	[μm]	[μm]	[mN/m]	[°]	[$\times 10^8$nm^3]
R_1	19	35	27	10	2
R_2	-/-	32.5	24	-/-	12
R_3	-/-	27.5	28	-/-	36

a_{crit} is reached. During the simulation, the predicted force F of the capillary bridge is constantly recorded. Gravitation is not taken into account in the simulation.

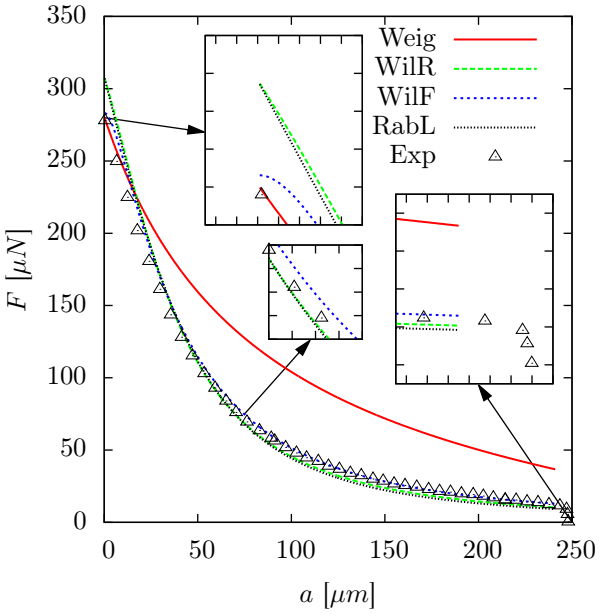

Figure 1: Comparison with Willett-experiments, [23, Fig. 1a, S. 9399], W_{11} (see Table 1)

In figures 1 and 2 results for the capillary force calculation in two different DEM simulations (setups W_{11} and R_1) are compared with the corresponding experimental data sets.

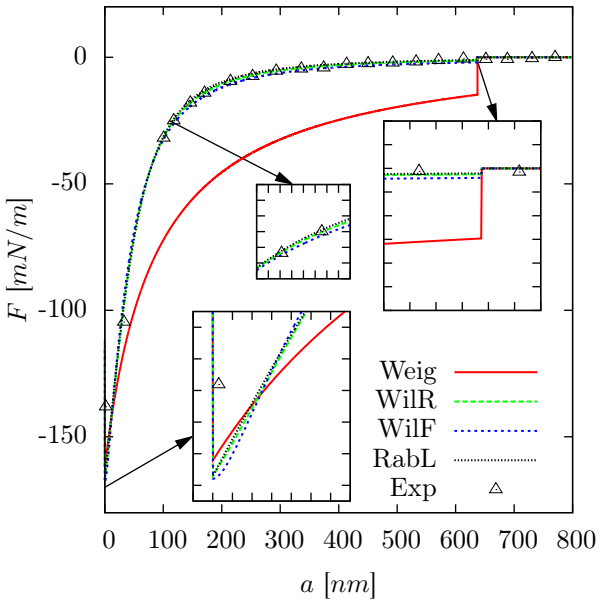

Figure 2: Comparison with Rabinovich-experiments, line 1, [17, Fig. 4, S. 10996], R_1 (see Table 1)

Obviously the overall agreement of the CBMs WilF, WilR and RabL to both experimental data sets from the micro- and the nano-scale is very good. Differences between the CBMs predictions and measurements are largest for small particle distances a, i. e. small bridge elongations.

On the contrary, the DEM simulations with CBM Weig fit only for small values of a to the experimental findings. Especially for the micro-scale setup W_{11} in figure 1, the CBM Weig is noticeable better in comparison to the other CBMs. However, the prediction quality of Weig CBM rapidly decreases for moderate and large values of a. Only the qualitative trend (nonlinear decreasing capillary force with increasing a) is captured with CBM Weig, but the capillary force values are markedly over-predicted.

An overview over the results from all DEM simulations (setups $W_{11} \ldots W_{33}$ and $R_1 \ldots R_3$) is given in figure 3. Here, relative capillary force values, defined as ratio from numerical and experimental force data, are given for three different bridge lengths $a_1 = 0$, $a_2 = 0.5\,a_{crit}$ and $a_3 = 0.95\,a_{crit}$. In general, the observations from setups W_{11} and R_1 are confirmed: whereas CBMs WillF, WillR and RabL match well to the measurements for most setups and all particle distances, Weig CBM gives only a satisfactory prediction for a small a values.

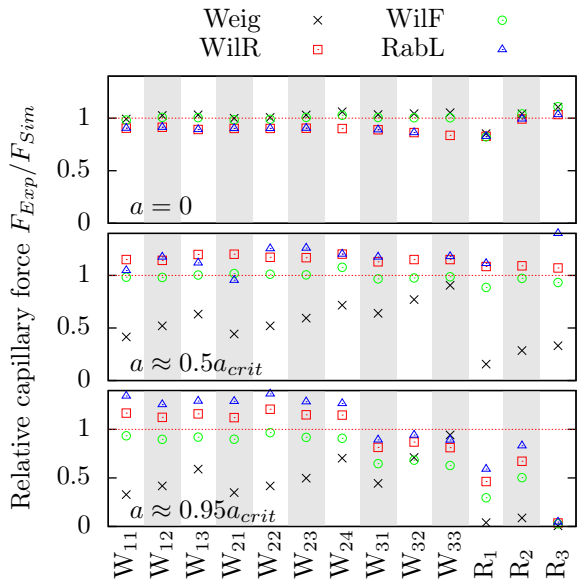

Figure 3: Capillary forces, obtained from simulations, are compared with experimental data (red dashed line)

4 CBM influence on macroscopic parameters

4.1 Shear cell setup

In a recent paper [20] the authors have demonstrated the visible influence of capillary forces on the hydrodynamic material parameters, e.g. viscosity, of wet granular matter in shearing motion. Now the effects of the different CBMs on these parameters are studied. Therefore, DEM-simulations of split-bottom ring-shear cell [2] are performed.

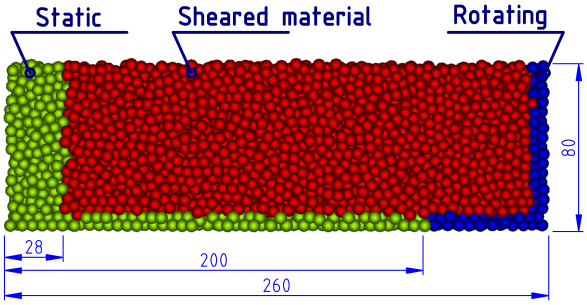

Figure 4: Setup of the split-bottom ring-shear cell in the DEM simulations. The center line of the rational symmetrical geometry is on the left, radii and height are given in mm.

The geometry of the packing in the shear cell is given in figure 4. The particle size of the monodisperse packing has been set to $R_{i=j} = 2.381$ mm, as in experiment W_{11} in table 1. The outer cylinder and the outer part of the bottom of the shear cell rotates with the period 100 s. The inner cylinder and the inner part of the bottom remains static.

The density of sheared particles is set to $\rho = 150$ kg/m^3 in order to get roughly the same mass of particles as in [20] and achieve comparable F_{norm}/F_{cap} relationship. The particle number for the simulation is nearly 200000. About 84% of all particles are in the region of the sheared material. The following model parameter are set: contact time $t_c = 5.4 \cdot 10^{-4}$ s, coefficient of restitution in normal and tangential directions $e_n = e_t = 0.83$, integration time step $\Delta t = 5.4 \cdot 10^{-6}$ s.

Every simulation has been run for a minimum of 5 s real flow time, corresponding to $\approx 10^6$ simulation time steps. The results showed, that such relatively low simulation time is enough to achieve steady state of the system. All simulations have been carried out on the HPC cluster of TU Bergakademie Freiberg. Although adding capillary bridges to the contact model of the DEM code increases the number of active contacts and complicates the calculation schema, it does not significantly decreases the calculation speed of the model. All simulations need nearly the same CPU time period with difference of only $\approx 10\%$. From every simulation, 15 snapshots are taken into account for averaging, see [20] for more details. The discrete averaging time step is 0.25 s.

4.2 Results and discussion

The dominating feature in the sheared granular material in the split-bottom shear cell is the shear band, i. e. a localized region where the granular material yields and flows [2]. In figure 5, the shear bands in the dry and two wet granular materials are compared. For the wet materials, resulting shear bands from the four CBMs Weig, WilF, WilR and RabL are shown.

Obviously, the center line and outer borderline of the shear band are shifted inwards in the wet materials. The displacement seems to depend on the liquid content as well. For larger liquid bridge volume (higher liquid content in the granular material), a stronger shift is observed. Regarding the four employed CBMs, we do not find a clear difference between the corresponding results (relocation of the shear bands).

The τ-p correlations give first insights into the macroscopic behavior of the granular material in the shear band. Figure 6 shows these correlations for dry and wet material with different liquid content. As expected, the correlations fit to the well-

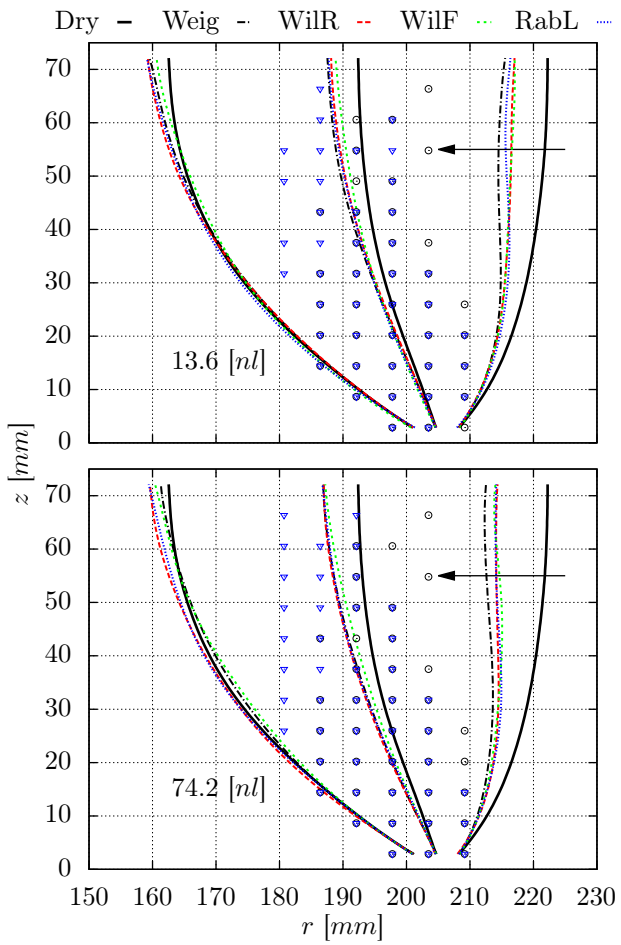

Figure 5: Shear bands in dry and wet materials. Black circles show the zones where $\dot{\gamma} > 0.12$ in dry material, blue triangles – in wet one.

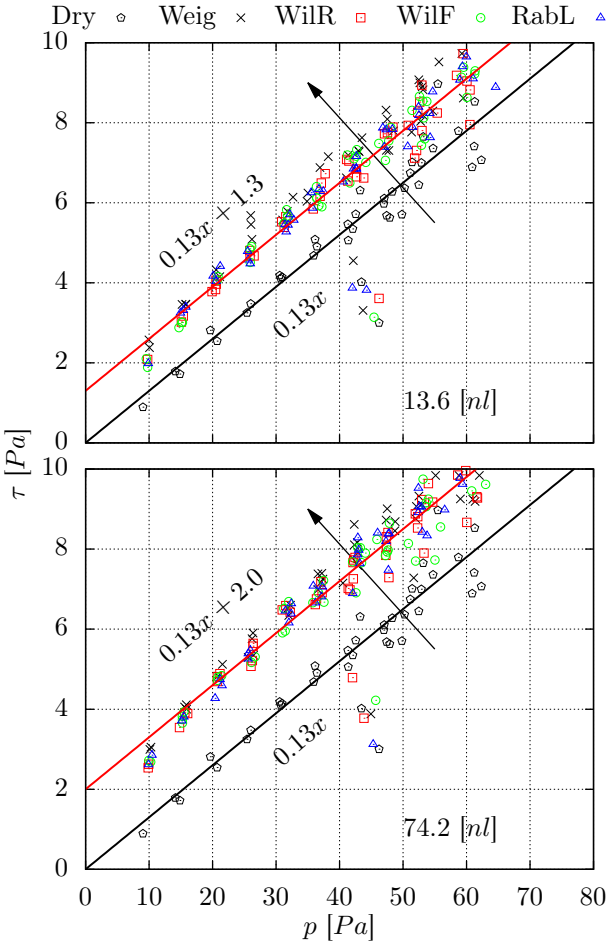

Figure 6: Shear stress τ plotted against pressure p where $\dot{\gamma} > 0.12$.

known constitutive law [12]

$$\tau = \mu\, p + c \tag{22}$$

with $\mu = 0.13$ for cohesive granular materials. Again, the parameters of the constitutive law depend significantly on the liquid content ($c_1 = 1.3\,Pa$ for $V_1 = 13.6$ nl, $c_2 = 2\,Pa$ for $V_2 = 74.2$ nl,), whereas the choice of the CBM has again no obvious influence on the macroscopic parameters (all points under red lines are very close to each other).

One more macro-parameter, which can be evaluated from the DEM results, is the torque M acting on the rotating part of the shear cell. The torque indicates indirectly the cohesive properties of the sheared material as well. It has been recorded during the whole rotating period of the simulations, time-averaged results are presented in figure 7. The results show the nonlinear dependency of the torque from the liquid content in the granular material. Again, the DEM simulations with the four different CBMs give nearly the same values of M.

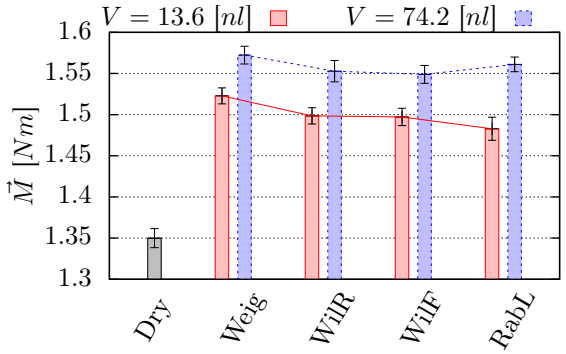

Figure 7: Average torque acting on rotating part of the shear cell during different simulation regimes.

We conclude from the results in figures 5 to 7, that the specific choice of the CBM has a minor importance for this type of granular flow. Changes in the overall flow field structure and corresponding hydrodynamic parameters correlate clearly with the liquid content in the granular material, but only

slightly with details of the capillary bridge force modelling.

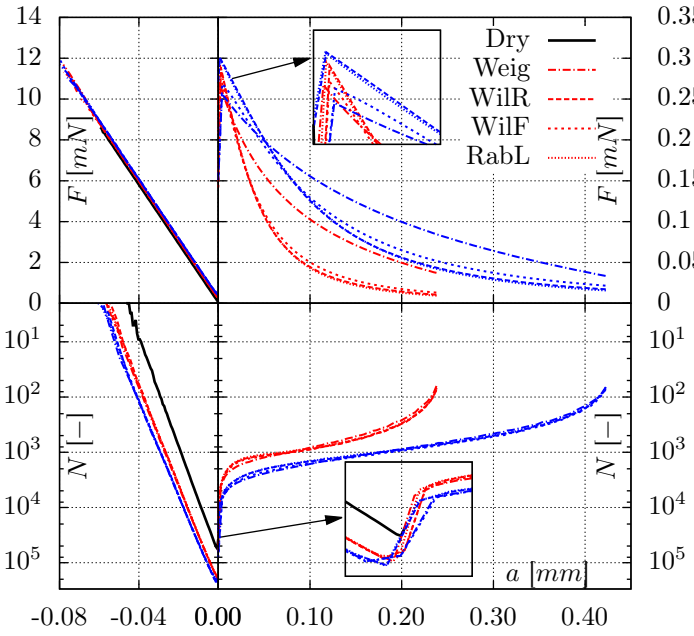

Figure 8: Contact distribution as a function of separation distance a (bottom row) for all CBMs and liquid volumes. Top row shows the force dependence on separation distance/penetration. Blue lines – 74.2 $[nl]$, red lines – 13.6 $[nl]$

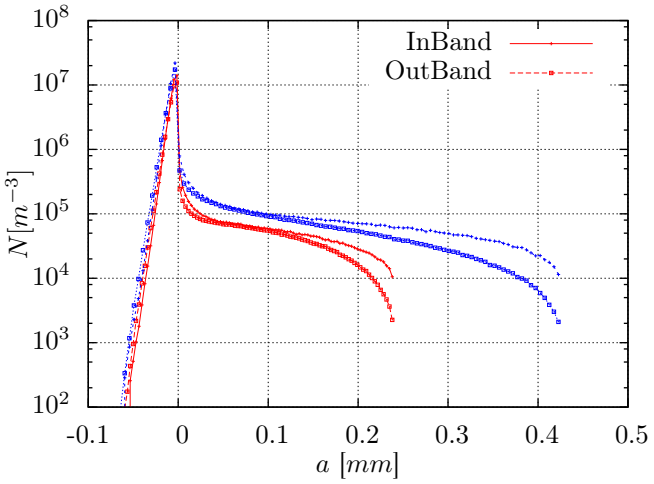

Figure 9: Contact distribution per volume in different parts of shear band (in and out) as a function of separation distance a for RabL CBM. Blue symbols – 74.2 $[nl]$, red lines – 13.6 $[nl]$

In order to understand these findings, we analyze the liquid bridge length distribution within the shear zone in more detail. Figure 8 gives the contact distance distribution in both dry (overlap) and wet (bridge length) contacts respectively. It is found, that most of the wet contacts have only short bridge length with respects to a_{crit}. Here, the capillary force prediction gives roughly the same values from all four investigated CBMs. Therefore, only small deviations are found for the macroscopic flow parameters.

Also the figure 8 (top row) shows distance-force dependencies, obtained from the shear cell simulations. Those curves are having absolutely the same dependency, like in a previous sphere-sphere simulations (figure 1). It proves the correct implementation of CBMs in the source code. Under the more dynamic conditions (increased cell rotation speed and thereby higher impact velocities), obtained curves can differ from static ones because of increased damping term of the total contact force.

The figure 9 shows the typical picture of contact distribution inside of shear band and out of it. To correctly compare contact numbers, here is introduced the contact number per volume. The diagram shows, that the relative number of contacts varies only for the range $a > 0.5a_{crit}$.

The relative contact number is smaller for the range $a > 0.5a_{crit}$ outside the shear band in compare to the region of shear band itself. The trend is independent on liquid volume. By other words in the shear band there are some more wet contacts, which are far away from each other due to higher velocity gradient.

5 Conclusion

In the paper four different kinds of capillary bridge models for DEM simulations are investigated. First, individual liquid bridges between a pair of spherical particles on the micro- and nano-scale are simulated. The predictions of the four capillary bridge models are compared to corresponding measurements. It is found, that the results of three capillary bridge models are very near to the experimental data. Contrary, one model gives only a reasonable qualitative representation of the capillary force development, but overestimates the force values strongly.

Then, the different capillary bridge models are employed in DEM simulations of wet granular material sheared in a split-bottom shear cell. Here, the flow field structure and corresponding macroscopic parameters clearly depend on the liquid content in the granular material. The differences, that have been found in the prediction of individual bridges on the micro-scale, are not visible on the macro-

scale. Therefore, the specific choice of the investigated capillary bridge model does not seem to have a marked influence on the prediction of the hydrodynamics of this type of granular flow.

Disclosure

The authors express their thanks to the Deutsche Forschungsgemeinschaft, which supported this work within the DFG/STW project "Hydrodynamic theory of wet particle systems" and cooperating institutions in this project.

Acknowledgments

Special thanks go to Prof. Stefan Luding for the helpful discussion.

References

[1] Derjaguin, B. Untersuchungen über die reibung und adhäsion, iv. *Kolloid-Zeitschrift 69*, 2 (1934), 155–164.

[2] Fenistein, D., van de Meent, J. W., and van Hecke, M. Universal and wide shear zones in granular bulk flow. *Phys. Rev. Lett. 92* (Mar 2004), 094301.

[3] Gabrieli, F., Lambert, P., Cola, S., and Calvetti, F. Micromechanical modelling of erosion due to evaporation in a partially wet granular slope. *International journal for numerical and analytical methods in geomechanics 36*, 7 (2012), 918–943.

[4] Gan, Y., Maggi, F., Buscarnera, G., and Einav, I. A particle-water based model for water retention hysteresis. *arXiv preprint arXiv:1307.5372* (2013).

[5] Herminghaus, S. Dynamics of wet granular matter. *Advances in Physics 54*, 3 (2005), 221–261.

[6] Iveson, S. M., Litster, J. D., Hapgood, K., and Ennis, B. J. Nucleation, growth and breakage phenomena in agitated wet granulation processes: a review. *Powder Technology 117*, 1 (2001), 3–39.

[7] Lambert, P. *Capillary forces in microassembly: modeling, simulation, experiments, and case study*. Springer, 2007.

[8] Lambert, P., Chau, A., Delchambre, A., and Régnier, S. Comparison between two capillary forces models. *Langmuir 24*, 7 (2008), 3157–3163.

[9] Lambert, P., and Regnier, S. Surface and contact forces models within the framework of microassembly. *Journal of Micromechatronics 3*, 2 (2004), 123–158.

[10] Lian, G., Thornton, C., and Adams, M. J. A theoretical study of the liquid bridge forces between two rigid spherical bodies. *Journal of Colloid and Interface Science 161*, 1 (1993), 138–147.

[11] Liu, P., Yang, R., and Yu, A. Dynamics of wet particles in rotating drums: Effect of liquid surface tension. *Physics of Fluids 23* (2011), 013304.

[12] Luding, S., and Alonso-Marroquín, F. The critical-state yield stress (termination locus) of adhesive powders from a single numerical experiment. *Granular Matter 13*, 2 (2011), 109–119.

[13] Mani, R., Kadau, D., and Herrmann, H. J. Liquid migration in sheared unsaturated granular media. *Granular Matter 15*, 4 (2013), 447–454.

[14] Mitarai, N., and Nori, F. Wet granular materials. *Advances in Physics 55*, 1-2 (2006), 1–45.

[15] Pietsch, W., and Rumpf, H. Haftkraft, kapillardruck, flüssigkeitsvolumen und grenzwinkel einer flüssigkeitsbrücke zwischen zwei kugeln. *Chemie Ingenieur Technik 39*, 15 (1967), 885–893.

[16] Pournin, L., Liebling, T. M., and Mocellin, A. Molecular-dynamics force models for better control of energy dissipation in numerical simulations of dense granular media. *Phys. Rev. E 65*, 1 (Dec 2001), 011302.

[17] Rabinovich, Y. I., Esayanur, M. S., and Moudgil, B. M. Capillary forces between two spheres with a fixed volume liquid bridge : Theory and experiment. *Langmuir 21*, 24 (2005), 10992–10997. eng.

[18] Radl, S., Kalvoda, E., Glasser, B. J., and Khinast, J. G. Mixing characteristics of wet granular matter in a bladed mixer. *Powder Technology 200*, 3 (2010), 171–189.

[19] Scholtès, L., Hicher, P.-Y., Nicot, F., Chareyre, B., and Darve, F. On the capillary stress tensor in wet granular materials.

International journal for numerical and analytical methods in geomechanics 33, 10 (2009), 1289–1313.

[20] Schwarze, R., Gladkyy, A., Uhlig, F., and Luding, S. Rheology of weakly wetted granular materials: a comparison of experimental and numerical data. *Granular Matter 15*, 4 (2013), 455–465.

[21] Soulie, F., Cherblanc, F., El Youssoufi, M. S., and Saix, C. Influence of liquid bridges on the mechanical behaviour of polydisperse granular materials. *International journal for numerical and analytical methods in geomechanics 30*, 3 (2006), 213–228.

[22] Weigert, T., and Ripperger, S. Calculation of the liquid bridge volume and bulk saturation from the half-filling angle. *Particle & Particle Systems Characterization 16*, 5 (1999), 238–242.

[23] Willett, C. D., Adams, M. J., Johnson, S. A., and Seville, J. P. K. Capillary bridges between two spherical bodies. *Langmuir 16*, 24 (2000), 9396–9405.

[24] Zhu, H., Zhou, Z., Yang, R., and Yu, A. Discrete particle simulation of particulate systems: theoretical developments. *Chemical Engineering Science 62*, 13 (2007), 3378–3396.

[25] Šmilauer, V., Catalano, E., Chareyre, B., Dorofeenko, S., Duriez, J., Gladky, A., Kozicki, J., Modenese, C., Scholtès, L., Sibille, L., Stránský, J., and Thoeni, K. *Yade Documentation*, 1st ed. The Yade Project, 2010. http://yade-dem.org/doc/.